THE JOURNAL OF PHYSICAL CHEMISTRY B

Article

pubs.acs.org/JPCB

Two-Dimensional HYSCORE Spectroscopy of Superoxidized Manganese Catalase: A Model for the Oxygen-Evolving Complex of Photosystem II

Christopher S. Coates,[†] Sergey Milikisiyants,[†] Ruchira Chatterjee,[†,§] Mei M. Whittaker,[‡] James W. Whittaker,[‡] and K. V. Lakshmi*[,†]

[†]Department of Chemistry and Chemical Biology and The Baruch '60 Center for Biochemical Solar Energy Research, Rensselaer Polytechnic Institute, Troy, New York 12180, United States

[‡]Division of Environmental and Biomolecular Systems, Institute of Environmental Health, Oregon Health & Science University, Portland, Oregon 97239-3098, United States

Supporting Information

ABSTRACT: The solar water-splitting protein complex, photosystem II (PSII), catalyzes one of the most energetically demanding reactions in Nature by using light energy to drive a catalyst capable of oxidizing water. The water oxidation reaction takes place at the tetranuclear manganese calcium-oxo (Mn_4Ca-oxo) cluster at the heart of the oxygen-evolving complex (OEC) of PSII. Previous studies have determined the magnetic interactions between the paramagnetic Mn_4Ca-oxo cluster and its environment in the S_2 state of the OEC. The assignments for the electron−nuclear magnetic interactions that were observed in these studies were facilitated by the use of synthetic dimanganese di-μ-oxo complexes. However, there is an immense need to understand the effects of the protein environment on the coordination geometry of the Mn_4Ca-oxo cluster in the OEC of PSII. In the present study, we use a proteinaceous model system to examine the protein ligands that are coordinated to the dimanganese catalytic center of manganese catalase from *Lactobacillus plantarum*. We utilize two-dimensional hyperfine sublevel correlation (2D HYSCORE) spectroscopy to detect the weak magnetic interactions of the paramagnetic dinuclear manganese catalytic center of superoxidized manganese catalase with the nitrogen and proton atoms of the surrounding protein environment. We obtain a complete set of hyperfine interaction parameters for the protons of a water molecule that is directly coordinated to the dinuclear manganese center. We also obtain a complete set of hyperfine and quadrupolar interaction parameters for two histidine ligands as well as a coordinated azide ligand, in azide-treated superoxidized manganese catalase. On the basis of the values of the hyperfine interaction parameters of the dimanganese model, manganese catalase, and those of the S_2 state of the OEC of PSII, for the first time, we discuss the impact of a proteinaceous environment on the coordination geometry of multinuclear manganese clusters.

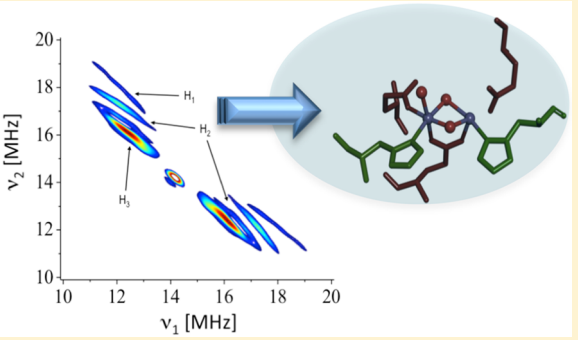

INTRODUCTION

In Nature, the solar water oxidation reaction is catalyzed by the photosynthetic reaction center, photosystem II (PSII), with remarkably high efficiency. PSII is a multisubunit membrane protein complex with the water oxidation reaction taking place in the oxygen-evolving complex (OEC) in the D1 polypeptide.[1−5] The OEC is comprised of a tetranuclear manganese-calcium-oxo (Mn_4Ca-oxo) cluster and surrounding amino acid residues. The catalytic cycle of the OEC involves five intermediate charge-storage (S-) states, S_0−S_4.[6] The S-state cycle begins in the dark-adapted S_1 state, and the OEC is progressively oxidized until the S_4 state which is followed by rapid release of molecular oxygen. Each S-state transition involves the absorption of a photon and the transfer of an electron or electron and proton. The structure of PSII has been studied by X-ray crystallography, spectroscopic, and biochemical methods.[7−13] While earlier crystallographic studies provided the structure of PSII,[14−17] these studies were unable to resolve the geometry of the OEC at high resolution due to possible radiation damage.[18−22] Extended X-ray absorption fine structure (EXAFS) spectroscopy has yielded accurate information on the relative position of the manganese and calcium ions of the Mn_4Ca-oxo cluster in the OEC.[23−26] In addition, limited structural information on the ligands of the Mn_4Ca-oxo cluster has been obtained by isotopic labeling of specific amino acid residues.[12,27−32] In a recent breakthrough, the structure of the OEC in the dark-adapted S_1 state has been solved at 1.9 Å resolution.[33] The X-ray crystal structure indicates that the OEC is comprised of three manganese ions, denoted as Mn1−Mn3,

Received: August 12, 2014

DOI: 10.1021/acs.jpcb.5b01602
J. Phys. Chem. B XXXX, XXX, XXX−XXX

and a calcium ion that forms a distorted cubane, while the fourth manganese ion, Mn4, is a "dangler" that is linked to the distorted cubane through a μ-oxo bridge. Additionally, there are two protein-derived ligands and four water molecules in the OEC that are thought to be directly coordinated to the manganese and calcium ions. Although the 1.9 Å resolution X-ray crystal structure has facilitated current proposals for the mechanism of the water oxidation reaction in the OEC of PSII, important structural questions still remain. In particular, the molecular and electronic structures of the higher S-state intermediates of the OEC need to be elucidated to gain insight into the mechanism of water oxidation.

Electron paramagnetic resonance (EPR) spectroscopy detects electronic interactions through the weak magnetic fields associated with nuclei in the environment of a paramagnetic center with unpaired electron(s). EPR spectroscopy has been particularly useful in characterizing the molecular and electronic structures of the OEC of PSII.[34−40] With the exception of the short-lived S_4 state, all of the S-state intermediates of the OEC have been detected by EPR spectroscopy.[35,41−49] The S_2 state intermediate has been the focus of the majority of the EPR spectroscopy studies on the OEC that have been published in the past two decades. The EPR spectrum of the S_2 state consists of a characteristic 18−22 multiline signal centered at an effective g value of 2.0 that corresponds to a net electron spin of $S = 1/2$.[50−54] However, an additional EPR signal centered at $g \sim 4.1$ has also been observed under a variety of sample preparation conditions.[40,55−60] It has been suggested that the $g \sim 4.1$ EPR signal corresponds to a high spin (electron spin $S = 5/2$) state of the OEC[40,57,58] and originates from either slight changes in the spin coupling scheme of the Mn_4Ca-oxo cluster[40,61] or a redistribution of valence states between the manganese ions within the cluster.[56] Interestingly, the two forms of the S_2 state are interconvertible by near-infrared irradiation at cryogenic temperatures.[55,56]

Conventional EPR spectroscopy has proven very useful in elucidating the structure of the S_2 state of the Mn_4Ca-oxo cluster in the OEC of PSII by detecting strong electron−nuclear hyperfine interactions with the four ^{55}Mn nuclei.[62−64] However, the electron−nuclear hyperfine interactions of the Mn_4Ca-oxo cluster in the S_2 state of the OEC with the nuclei in the first or second coordination sphere are weaker (by more than an order of magnitude) and are completely masked by the magnetic field inhomogeneity across the sample. In this case, advanced techniques, including electron nuclear double resonance (ENDOR), electron-spin-echo envelope modulation (ESEEM), and two-dimensional (2D) hyperfine sublevel correlation (HYSCORE) spectroscopy, are required to overcome the inhomogeneity problem. The hyperfine interactions of the Mn_4Ca-oxo cluster in the S_2 state of the OEC with the nitrogen atoms of surrounding amino acid residues have previously been determined by multifrequency ENDOR,[12] ESEEM,[65−67] and 2D HYSCORE spectroscopy.[9,68] There are also several proton hyperfine interactions of the Mn_4Ca-oxo cluster in the S_2 state of the OEC that have been measured by ENDOR,[12,35,41,69,70] ESEEM,[35,71] and 2D HYSCORE spectroscopy.[8,72] Although an abundance of spectroscopic information has been obtained using high-resolution EPR spectroscopic techniques, information on the molecular and electronic structures of the OEC is limited, mainly due to the complexity of the OEC that makes it difficult to correlate the spectroscopic observations with structural conclusions. Thus, there is an urgent need for spectroscopic measurements of simple models that mimic the Mn_4Ca-oxo cluster in the OEC of PSII.

Several synthetic mixed-valence Mn(III)−Mn(IV) dimanganese models have been used to mimic some of the features of the Mn_4Ca-oxo cluster in the S_2 state of the OEC.[73,74] In particular, the electron−nuclear hyperfine interactions of mixed-valence Mn(III)−Mn(IV) centers with the protons from organic ligands[75−77] and directly coordinated water molecules[76,78] have been previously characterized. Additionally, the hyperfine interactions of directly coordinated nitrogen atoms have been measured for Mn(III)[77,79,80] and Mn(IV)[80] ions in different coordination geometries. However, it is important that, in comparison with the synthetic dimanganese models, the spectroscopic properties of the OEC are sensitive to features in the surrounding ligand environment and are significantly affected by distortions of the coordination geometry due to steric interactions within the Mn_4Ca-oxo cluster.[52,81−84]

The dimanganese-containing catalase in its "superoxidized" mixed-valence Mn(III)−Mn(IV) state has been used as a proteinaceous model of the Mn_4Ca-oxo cluster in the OEC of PSII.[85−87] In contrast with the synthetic dimanganese models, superoxidized manganese catalase mimics important features of the protein environment of the Mn_4Ca-oxo cluster in the OEC, with coordination by protein side chains (including two histidine residues) and a water molecule.[88] This makes manganese catalase a particularly suitable model for the Mn_4Ca-oxo cluster in the OEC of PSII. The hyperfine interactions of one of the nitrogen atoms and surrounding protons with the dimanganese center of manganese catalase have previously been resolved by ESEEM[89] and ENDOR spectroscopy.[86,90] In recent multifrequency ESEEM spectroscopy studies, the hyperfine interactions of both of the directly coordinated nitrogen atoms of the histidine ligands have been resolved spectroscopically.[87] Despite the spectroscopic data that is available, the oxidation state of the manganese ions and the coordination geometry of the manganese ions in the superoxidized state of the dimanganese center of manganese catalase remain unclear.

In this report, we provide a detailed study of superoxidized *Lactobacillus plantarum* (LP) manganese catalase by 2D HYSCORE spectroscopy. We determine, for the first time, a complete set of electron−nuclear hyperfine interactions of the dimanganese center of manganese catalase with the protons of the directly coordinated water molecule and the proximal proton of one of the histidine ligands. In addition, we examine the binding of azide to the dimanganese center of manganese catalase that allows for direct observation of the nitrogen atoms of the azide ion. The hyperfine parameters for the protons and nitrogen atoms that are obtained in this study provide exclusive insight on the electronic structure of both manganese catalase and the OEC of PSII.

MATERIALS AND METHODS

Preparation of Manganese Catalase from *Lactobacillus plantarum*. *L. plantarum* (NCDO 1193) (LP) was used for high-level expression of wild-type recombinant LP manganese catalase. Protein expression and manganese catalase purification were performed as previously described.[91] The dimanganese catalytic site of manganese catalase was converted to the mixed-valence Mn(III)−Mn(IV) superoxidized state using a modification of previously published procedures.[92,93] As-isolated LP manganese catalase (0.1 mM active sites, in 50 mM potassium

DOI: 10.1021/acs.jpcb.5b01602
J. Phys. Chem. B XXXX, XXX, XXX−XXX

phosphate buffer, pH 7) was subjected to redox cycling by dialysis against the same buffer containing 0.1 mM hydroxylamine sulfate and 0.1 mM hydrogen peroxide for 4 h at 4 °C, followed by dialysis against fresh buffer without redox agents. Spectroscopic samples containing 0.3 mM manganese catalase active sites were prepared in 50 mM potassium phosphate buffer (pH 6.0), 0.1 mM EDTA, and 25% (v/v) glycerol. Deuterium exchanged manganese catalase was prepared by incubation of the protein in buffer prepared in D_2O. Azide-treated manganese catalase was prepared by incubating protein in protonated buffer with 15 mM sodium azide.[88,93,94] All of the manganese catalase samples were then loaded into a 4 mm quartz tube and frozen at 77 K in liquid nitrogen.

Pulsed EPR Spectroscopy. The X-band EPR spectra were recorded on a custom-built cw/pulsed X-band Bruker Elexsys 580 spectrometer (Bruker BioSpin, Billerica, MA). The pulsed EPR spectroscopy measurements were conducted with a flex-line split ring resonator ER-4118X-MS5 (Bruker BioSpin, Billerica, MA), and a dynamic continuous-flow cryostat CF935 (Oxford Instruments, Oxfordshire, UK) was used for the cryogenic measurements. All of the spectra were acquired at 5 K.

A six-pulse HYSCORE sequence was used for the acquisition of the 2D HYSCORE spectra.[95,96] For the six-pulse HYSCORE sequence, the echo amplitude was measured with the pulse sequence $(\pi/2)_y$-τ_1-$(\pi)_y$-τ_1-$(\pi/2)_x$-t_1-$(\pi)_x$-t_2-$(\pi/2)_x$-τ_2-$(\pi)_x$-τ_2-$(\text{echo})_x$. The interpulse delays were defined as the difference between the starting points of the pulses. The echo intensity was obtained by integration over the 8 ns detector gate and measured as a function of t_1 and t_2, where t_1 and t_2 were incremented in steps of 16 ns from the initial values of 24 and 32 ns, respectively. Equal amplitude pulses of 8 ns for the $\pi/2$ pulse and 16 ns for the π pulse were used to record a 256 × 256 matrix. The 8 ns time difference between the initial value of the time delays, t_1 and t_2, and the $\pi/2$ and π pulses was used to account for the difference in length between the $\pi/2$ and π pulses to obtain symmetric spectra. The blind spot pattern in a six-pulse 2D HYSCORE spectrum is determined by the τ_1 and τ_2 delays. The τ_1 delay has been chosen to be 24 ns to avoid blind spots in the entire spectral region. The τ_2 delay has been chosen to be 136 ns to avoid resonator ring down and suppress matrix protons. The application of an eight-step phase cycling procedure was used to eliminate the unwanted echoes.[95] The operating microwave frequency of the pulsed resonator was 9.34, 9.41, and 9.40 GHz for manganese catalase in protonated buffer, deuterated buffer, and azide-treated samples, respectively. The 2D HYSCORE spectra were recorded at magnetic field positions corresponding to the maximum of the electron-spin-echo signal: 332.8, 335.3, and 335.2 mT for manganese catalase in protonated buffer, deuterated buffer, and azide-treated samples, respectively.

The time domain 2D ^{14}N HYSCORE data was processed using MATLAB R2012a. The echo decay was eliminated by a low order polynomial baseline correction and tapered with a Gaussian function. Prior to 2D Fourier transformation, the data was zero filled to a 2048 × 2048 matrix and the magnitude spectra were calculated. The 2D ^{14}N HYSCORE spectra are presented as contour plots using the "contour" function of the MATLAB R2012a software.

The position of the cross-peaks in the 2D HYSCORE spectrum is determined by the hyperfine interactions and depends on the orientation of the paramagnetic center with respect to the external magnetic field. Thus, cross-peaks form extended ridges in disordered samples, such as frozen solutions. The cross-peaks appear in pairs where the peaks are symmetrically displaced from the main diagonal, since the populations of the two spin manifolds under resonance are approximately equal at moderate temperatures. Thus, for every cross-peak or ridge in the spectrum, there is a ridge that is located symmetrically with respect to the main diagonal and carries identical spectroscopic information. For nuclei with spin $I = 1/2$, such as protons, the ridges represent the segments of an ellipsoid that is determined by the relation between nuclear Zeeman and hyperfine interactions. In frequency-squared coordinates, the segments of an ellipsoid are transformed into segments of a straight line. The isotropic, A_{iso}, and anisotropic, T, components of the hyperfine interaction can be determined from the slope and the intercept of the straight line using the following equations[97]

$$T = \pm\sqrt{\frac{16}{9(1-Q)}\left\{G + \frac{4{\nu_I}^2 Q}{1-Q}\right\}} \quad (1)$$

$$A_{iso} = \pm 2\nu_I \frac{1+Q}{1-Q} - \frac{T}{2} \quad (2)$$

where ν_I is the nuclear Zeeman frequency for the given magnetic field, Q is the slope, and G is the intercept of the straight line. In principle, the sign in eqs 1 and 2 is positive for a paramagnetic center containing a single metal ion, since T is determined by the through space dipole−dipole interaction. However, in metal clusters, the electron spins of the individual paramagnetic metal ions are coupled with each other and an opposite orientation of the electron spin with respect to external magnetic field is possible, allowing for the presence of a negative anisotropic coupling. For the antiferromagnetically coupled mixed-valence Mn(III)−Mn(IV) dimanganese center of manganese catalase, a positive coupling is induced by the Mn(III) ion and a negative coupling by the Mn(IV) ion. Thus, for the nuclei that are located in the proximity of the Mn(III) ion, a positive sign should be taken into account in eqs 1 and 2. To estimate the errors of the hyperfine parameters, we measured the admissible variations of values of the slope and the intercept, Q and G, respectively, by considering various points in the middle of the ridges and the variation amplitude of the hyperfine parameter was taken as its error bar.

For nuclei with spin $I = 1$, such as ^{14}N, each electron spin manifold is split into three nuclear substates. Thus, for a given EPR transition, there are several types of cross-peaks that can be observed in the 2D HYSCORE spectrum. There are single quantum−single quantum (SQ−SQ), single quantum−double quantum (SQ−DQ), and double quantum−double quantum (DQ−DQ) correlations that are possible. The frequency of SQ transitions usually has a strong dependence on the orientation of the paramagnetic center that results in cross-peaks or ridges that are broad with low intensity. In contrast, DQ−DQ transitions are highly localized and are easily detected by 2D HYSCORE spectroscopy. The position of the DQ−DQ correlations is determined by the following equations

$$\nu_\alpha = \mp 2\sqrt{(\nu_I + A/2)^2 + K^2(3+\eta^2)} \quad (3)$$

$$\nu_\beta = \mp 2\sqrt{(\nu_I - A/2)^2 + K^2(3+\eta^2)} \quad (4)$$

where ν_I is the nuclear Zeeman frequency, A is the electron−nuclear hyperfine coupling constant, $K = e^2qQ/4\hbar$ where Q is

DOI: 10.1021/acs.jpcb.5b01602
J. Phys. Chem. B XXXX, XXX, XXX−XXX

the quadrupole moment interacting with the electric field gradient q, and η is the asymmetry parameter of the quadrupolar tensor.

RESULTS

Electron-Spin-Echo Field-Sweep EPR Spectrum of Manganese Catalase. Figure 1 displays the electron-spin-echo field-sweep EPR spectrum of manganese catalase in protonated buffer. The EPR spectrum consists of ~16 pronounced peaks that are centered at a g value of ~2.0. This spectrum is typical of a dimanganese Mn(III)−Mn(IV) center with antiferromagnetically coupled paramagnetic manganese ions.[38,39,98,99] The EPR spectrum is in agreement with previous reports in the literature.[87,100−102] There is no evidence for residual Mn(II) species in the field-sweep EPR spectrum.

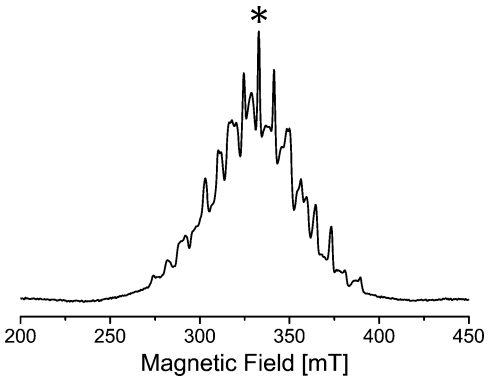

Figure 1. Electron-spin-echo field-sweep EPR spectrum of superoxidized manganese catalase in protonated buffer. The magnetic field position that was used for the 2D ^{1}H and ^{14}N HYSCORE spectroscopy measurements is marked with an asterisk.

2D HYSCORE Spectroscopy of Manganese Catalase in Protonated Buffer. The weak electron−nuclear hyperfine interactions that are unresolved in the electron-spin-echo field-sweep spectrum of manganese catalase (Figure 1) due to inhomogeneous line broadening can be detected through the application of 2D HYSCORE spectroscopy. A 2D HYSCORE spectrum measures the electron−nuclear hyperfine interactions of two electron spin manifolds as cross-correlation peaks in two-dimensional frequency space.[103] The electron spin manifolds that are detected by 2D HYSCORE spectroscopy correspond to the transition that is in resonance with the microwave irradiation at a specific magnetic field position.

Figure 2A shows the complete 2D HYSCORE spectrum of manganese catalase in protonated buffer measured at the magnetic field corresponding to the maximum of the field-sweep EPR spectrum (marked with an asterisk in Figure 1). Two distinct groups of multiple cross-peaks or ridges are observed in the spectrum. The first group of ridges, centered at ~14.2 MHz in the (+, +) quadrant of the 2D HYSCORE spectrum, arises from the electron−nuclear hyperfine interactions with multiple protons that are in the vicinity of the paramagnetic Mn(III)−Mn(IV) center of manganese catalase. The second group of ridges, consisting of two pairs of pronounced peaks in the (−, +) quadrant of the spectrum, arises from hyperfine interactions of the paramagnetic Mn(III)−Mn(IV) center of manganese catalase with two ^{14}N atoms.

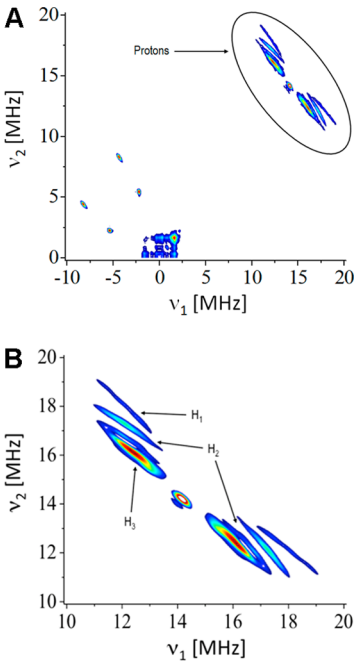

Figure 2. (A) The complete 2D HYSCORE spectrum of superoxidized manganese catalase in protonated buffer. (B) The 2D ^{1}H HYSCORE spectrum of superoxidized manganese catalase in protonated buffer.

The first group of ridges corresponding to protons is shown in detail in Figure 2B. There are four pairs of ridges that arise from electron−nuclear hyperfine interactions of the dinuclear manganese center with proximal protons. There is an additional feature that is located on the main diagonal that is due to hyperfine interactions with the matrix protons. The first pair of ridges in the (+, +) quadrant of the 2D HYSCORE spectrum displays the largest shift from the antidiagonal that crosses the main diagonal at the proton Zeeman frequency (14.7 MHz). This shift is caused by the anisotropic component of the hyperfine interaction, T, and is proportional to T^2. This pair of ridges reflects hyperfine interactions with a group of proton(s), H_1, that are located in close proximity of the Mn(III)−Mn(IV) center of manganese catalase. There are two other pairs of ridges that are moderately shifted from the antidiagonal and are on the same straight line in frequency-squared coordinates (Figure 1S in the Supporting Information). These ridges arise from the hyperfine interaction of the Mn(III)−Mn(IV) center with a second group of proton(s), H_2. The reason that we observe two pairs of ridges with the second group of proton(s) is that these two ridges are located on different sections of the main diagonal. These ridges belong to a common ridge that was split by the experimental blind spot at a proton Zeeman frequency of 14.7 MHz. These two ridges are also located on the same straight line in frequency-squared coordinates, as they are part of the same extended ridge that was split by the blind spot. Finally, there is a pair of ridges that is much broader and is very close to the antidiagonal in Figure 2B. These ridges are curved in frequency-squared coordinates, indicating that they arise from multiple hyperfine interactions with a group of protons, H_3, with overlapping spectra.

By determining the position of the ridges on the 2D HYSCORE spectrum and using eqs 1 and 2, we obtain the isotropic and anisotropic components, A_{iso} and T, respectively, of the hyperfine interaction for the H_1 and H_2 groups of

DOI: 10.1021/acs.jpcb.5b01602
J. Phys. Chem. B XXXX, XXX, XXX−XXX

protons (please see the Materials and Methods section). The values of A_{iso} and T are presented in Table 1. Both H_1 and H_2

Table 1. Proton Hyperfine Parameters for Superoxidized Manganese Catalase That Are Obtained from the 2D ^{1}H HYSCORE Spectroscopy Measurements in Protonated Buffer[a]

group of protons	A_{iso} (MHz)	T (MHz)
H_1	±3.3 (±0.3)	±6.7 (±0.3)
H_2	±1.0 (±0.2)	±5.5 (±0.2)

[a]The respective error bars are indicated in parentheses.

have a significant anisotropic hyperfine component, T, of ±6.7 and ±5.5 MHz, respectively. This indicates that both H_1 and H_2 are close to the paramagnetic Mn(III)−Mn(IV) center of manganese catalase. The H_1 group of protons has a large isotropic hyperfine interaction, A_{iso}, of ±3.3 MHz, reflecting the Fermi contact interaction for a directly coordinated ligand. This indicates that the proton(s) are associated with an atom that is covalently bound to one of the manganese ions of the Mn(III)−Mn(IV) center. In contrast, the isotropic component of the hyperfine interaction with the H_2 group of protons is small, A_{iso} = ±1.0 MHz, which indicates that these proton(s) are several bonds removed from the paramagnetic Mn(III)−Mn(IV) center.

Figure 3 shows the 2D ^{14}N HYSCORE spectrum of manganese catalase in protonated buffer. There are two pairs

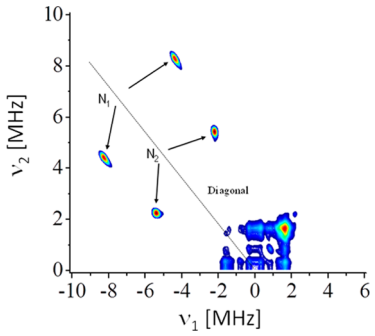

Figure 3. 2D ^{14}N HYSCORE spectrum of superoxidized manganese catalase in protonated buffer.

of ridges that are symmetrically displaced from the main diagonal in the (−, +) quadrant of the spectrum. These ridges arise from hyperfine interactions of the paramagnetic Mn(III)−Mn(IV) center with two magnetically distinct ^{14}N atoms, N_1 and N_2. The separation between the two symmetric ridges of each pair is approximately 4 times the ^{14}N Zeeman frequency (ν_I = 1.02 MHz), indicating that the observed features are DQ−DQ correlations. The location of the ridges is almost entirely determined by the relationship between the isotropic hyperfine coupling, nuclear Zeeman frequency, and quadrupolar parameter, K. Typically, anisotropic hyperfine interactions lead to an extension of the ridges along the main diagonal. Thus, the highly localized ridges in Figure 3 indicate that the anisotropic component, T, is much smaller than the isotropic component, A_{iso}, of the hyperfine interaction with the N_1 and N_2 nitrogen atoms.

The values of A_{iso} and $K^2(3 + \eta^2)$ that are obtained by using eqs 3 and 4 are presented in Table 2. The quadrupolar parameters are determined by the local electric field gradient

Table 2. Nitrogen Hyperfine and Quadrupolar Parameters for Superoxidized Manganese Catalase That Are Obtained from the 2D ^{14}N HYSCORE Spectroscopy Measurements in Protonated Buffer[a]

nitrogen atom	A_{iso} (MHz)	$K^2(3 + \eta^2)$ (MHz^2)
N_1	±6.0 (±0.5)	0.9 (±0.02)
N_2	±3.0 (±0.2)	1 (±0.02)

[a]The respective error bars are indicated in parentheses.

that is directly related to the chemical environment of the nucleus. For the nitrogen atoms N_1 and N_2, the quadrupolar parameter is nearly identical with the value of $K^2(3 + \eta^2)$ of 0.9 and 1.0 MHz^2, respectively. This indicates a similar chemical nature for the N_1 and N_2 nitrogen atoms. In contrast, the isotropic component of the hyperfine interaction, A_{iso}, for N_1 is twice the value of A_{iso} for N_2, ±6.0 and ±3.0 MHz, respectively, indicating distinct magnetic interactions of the Mn(III)−Mn(IV) center with the two nitrogen atoms N_1 and N_2.

To further characterize the three groups of protons, H_1−H_3, that magnetically interact with the Mn(III)−Mn(IV) center of manganese catalase, we measured the 2D ^{1}H HYSCORE spectrum of superoxidized manganese catalase in deuterated buffer. The complete 2D HYSCORE spectrum is shown in Figure 2S (Supporting Information). Upon comparison of the 2D HYSCORE spectrum of manganese catalase in protonated (Figure 2) and deuterated (Figure 2S, Supporting Information) buffer, differences are observed in the spectral region containing the cross-peaks arising from proton hyperfine interactions. In the 2D ^{1}H HYSCORE spectrum of manganese catalase in deuterated buffer shown in Figure 4, the ridges arising from

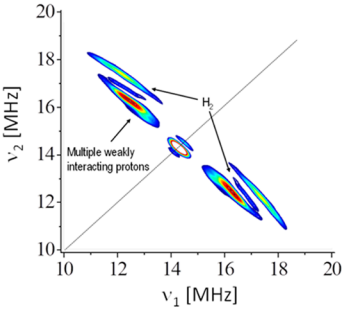

Figure 4. 2D ^{1}H HYSCORE spectrum of superoxidized manganese catalase in deuterated buffer.

hyperfine interactions with the H_2 group of proton(s) are unaffected by deuterium exchange. However, the ridges due to the hyperfine interaction with the H_1 group of proton(s) are absent in this spectrum, indicating that the proton(s) in the H_1 group are exchangeable with deuterons in the solvent.

As demonstrated by a recent X-ray crystal structure of manganese catalase in the presence of sodium azide, the water molecule that is directly coordinated to the dinuclear manganese center is replaced by an azide ion.[88] Thus, the directly coordinated nitrogen atom of the azide ligand is an excellent probe to refine the electronic structure of superoxidized manganese catalase and specifically address the coordination geometry of the manganese ion that coordinates both the His69 residue and the water ligand in the active site. Figure 3S (Supporting Information) displays the electron-spin-echo field-sweep EPR spectrum of azide-treated manganese catalase. The EPR spectrum of azide-treated manganese

DOI: 10.1021/acs.jpcb.5b01602
J. Phys. Chem. B XXXX, XXX, XXX−XXX

catalase displays ~16 peaks that are centered at a g value of ~2.0 which is similar to the EPR spectrum of untreated manganese catalase. This spectrum is typical of a dimanganese Mn(III)−Mn(IV) center with antiferromagnetically coupled paramagnetic manganese ions.[38,39,98,99] The EPR spectrum is in agreement with previous reports in the literature.[89] The complete 2D HYSCORE spectrum of azide-treated superoxidized manganese catalase is shown in Figure 4S (Supporting Information). Shown in Figure 5S (Supporting Information) and Figure 5 are the 2D ^{1}H and ^{14}N HYSCORE spectra of

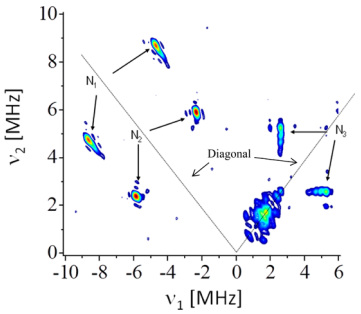

Figure 5. 2D ^{14}N HYSCORE spectrum of superoxidized azide-treated manganese catalase in protonated buffer.

azide-treated manganese catalase, respectively. The complete 2D HYSCORE spectrum of azide-treated manganese catalase is similar to the spectrum that was measured in the absence of azide with two essential differences: the ridges from the hyperfine interaction with the H_1 group of protons are absent, and an additional pair of cross-peaks, N_3, appear in the (+, +) quadrant of the spectrum. There are minor shifts of the ridges that arise from the hyperfine interactions of the Mn(III)−Mn(IV) center with the proton and nitrogen atoms, H_2, N_1, and N_2, respectively. This indicates small perturbations of the electronic structure of the Mn(III)−Mn(IV) center upon azide binding.

The hyperfine parameters that are obtained for the nitrogen atoms, N_1, N_2, and N_3, in azide-treated manganese catalase are presented in Table 3. There is a small increase in the isotropic

Table 3. Nitrogen Hyperfine and Quadrupolar Parameters for Superoxidized Azide-Treated Manganese Catalase That Are Obtained from the 2D ^{14}N HYSCORE Spectroscopy Measurements in Protonated Buffer[a]

nitrogen atom	A_{iso} (MHz)	$K^2(3 + \eta^2)$ (MHz^2)
N_1	±6.4 (±0.3)	0.9 (±0.02)
N_2	±3.5 (±0.2)	0.9 (±0.02)
N_3	±2.5 (±0.2)	1.6 (±0.02)

[a]The respective error bars are indicated in parentheses.

component, A_{iso}, of the hyperfine interaction with the nitrogen atoms N_1 and N_2 of ±6.4 and ±3.5 MHz, respectively, while the corresponding quadrupolar parameters remain virtually unchanged. The value of A_{iso} for the N_3 nitrogen atom is small (±2.5 MHz) in comparison with the A_{iso} values of the N_1 and N_2 nitrogen atoms. In contrast, the quadrupolar parameter $K^2(3 + \eta^2)$ of 1.6 MHz^2 is nearly twice the quadrupolar parameter of 0.9 MHz^2 that is obtained for the nitrogen atoms N_1 and N_2. The small value of A_{iso} is probably the reason that the nitrogen atom N_3 has escaped detection in previous 1D ESEEM studies.[89]

DISCUSSION

Assignment of the ^{1}H and ^{14}N Hyperfine Interactions of Manganese Catalase. In order to assign the hyperfine parameters that are obtained from the 2D ^{1}H and ^{14}N HYSCORE spectra, we use the X-ray crystal structure of oxidized Mn(III)−Mn(III) manganese catalase[88] and previous spectroscopic studies of superoxidized manganese catalase[86,87,90] and related model systems.[75−78,80] There are two manganese ions, Mn1 and Mn2, in the active site of manganese catalase. The manganese ion, Mn1, is coordinated by the histidine and glutamic acid residues, His69 and Glu35, respectively, and a single water molecule. The manganese ion, Mn2, is coordinated by the histidine and glutamic acid residues, His181 and Glu148, respectively. In addition, the two μ-oxo oxygen atoms and the side chain of the glutamic acid, Glu66, serve as bridging ligands between the Mn1 and Mn2 ions.

The magnitudes of the isotropic and anisotropic components of the hyperfine interaction with the H_1 group of proton(s) (Table 1) are in agreement with the hyperfine parameters that were previously observed for protons of a terminal water ligand that is bound to a Mn(III) ion in the [MnIII/IV[2-OH-3,5-Cl_2-(salpn)]$_2$(THF)]$^+$ complex (where salpn = *N*,*N*′-bissalicylidene-1,3-diamino-2-hydroxypropane)[78] (MnSalpn) and the [H_2O(terpy)-Mn^{III}(μ-O)$_2$$Mn^{IV}$(terpy)$OH_2$]($NO_3$)$_3$] complex (where terpy = 2,2′:6′,2″-terpyridine) (MnTerpy).[76] As observed in Figures 4 and 5S (Supporting Information), the ridges that arise from the hyperfine interaction with the exchangeable group of proton(s), H_1, are absent in the presence of azide. Thus, we assign the H_1 group of proton(s) to the water ligand that is coordinated to the Mn1 ion that is in the Mn(III) oxidation state. Since the dominant contribution to the hyperfine interaction of the H_1 group of proton(s) is from the Mn(III) ion, both T and A_{iso} have positive signs. The values of A_{iso} = 3.3 MHz and T = 6.7 MHz yield a hyperfine tensor with principal values of [−3.4, −3.4, 16.7] MHz. The largest value of the principal component of the hyperfine tensor of 16.7 MHz is in agreement with the proton coupling of 17.2 MHz that was previously detected by ENDOR spectroscopy[86] which was assigned to the water ligand bound to the Mn1 ion in the Mn(III) oxidation state. Interestingly, the authors had also observed another coupling of 12.2 MHz which was assigned to the second proton of the same water ligand that was thought to be located further away from the Mn(III) ion. We do not observe a pronounced asymmetry between the two protons of the water ligand. The narrow shape of the ridges that corresponds to the hyperfine interaction with the H_1 group proton(s) indicates approximate magnetic equivalence of the water protons and distances to the Mn1 ion. However, there is a possibility that a second proton has escaped detection in the present study.

Solely on the basis of the hyperfine parameters that are obtained here, there are two possible assignments for the H_2 group of proton(s). First, H_2 is the proximal proton of the His69 ligand or, second, the proton of the water ligand that is bound to the Mn(IV) ion. The second assignment would imply that the oxidation states may be switched between the two manganese ions. Since the H_2 group of proton(s) is not affected by deuterium exchange, we exclude the second possibility, and we unambiguously assign the H_2 group of proton(s) to the proximal protons of the His69 ligand. Again, similar to the H_1 group of protons, the positive signs in eqs 1 and 2 yield values

DOI: 10.1021/acs.jpcb.5b01602
J. Phys. Chem. B XXXX, XXX, XXX−XXX

of T and A_{iso} of 5.5 and −1.0 MHz, respectively, and a corresponding hyperfine tensor of [−6.5, −6.5, 10] MHz.

In contrast with the H_1 and H_2 groups of protons, the assignment of the hyperfine interaction with the nitrogen atoms N_1 and N_2 is nontrivial. The magnitude of the isotropic component of the hyperfine interaction indicates that the nitrogen atoms are directly coordinated to the paramagnetic Mn(III)−Mn(IV) center. Although His69 and His181 are the only ligands to the dimanganese core that contain nitrogen atoms, the specific assignment of N_1 and N_2 being coordinated to a Mn(III) or Mn(IV) center is not obvious. In order to distinguish between these two possibilities, we consider the spectroscopic properties of nitrogen ligands of Mn(III) and Mn(IV) ions that are reported in the literature. In previous 2D HYSCORE spectroscopy investigations, we have measured the hyperfine interactions of axial and equatorial nitrogen ligands that are coordinated to both Mn(III) and Mn(IV) ions.[80] Additional hyperfine parameters are also available in the literature for axial nitrogen ligands coordinated to a Mn(III) ion.[12,79,87,90] It is observed that there is a large asymmetry in the magnetic properties of the axial and equatorial nitrogen ligands of a Mn(III) ion. While the isotropic component of the electron−nuclear hyperfine interaction was found to be large, $|A_{iso}| \geq 9$ MHz, for axial coordination to a nitrogen ligand, very weak couplings, $|A_{iso}| \leq 2$ MHz, have been observed for equatorial coordination. In contrast, the Mn(IV) ion has a much larger degree of symmetry and both axial and equatorial nitrogen ligands are found to have similar hyperfine parameters of $|A_{iso}| \sim 3-4$ MHz. All of the quadrupolar couplings were previously estimated to be similar to a value of ∼1 MHz^2 for $K^2(3 + \eta^2)$, except for the equatorial nitrogen ligands of a Mn(III) ion where the quadrupolar coupling was found to be 2 times larger with a value of ∼2 MHz^2 for $K^2(3 + \eta^2)$. The values of A_{iso} of N_1 of ±6.0 and ±6.4 MHz in the absence and presence of azide, respectively, are much larger than the values of A_{iso} that were previously detected for nitrogen ligands of a Mn(IV) ion. The values of A_{iso} are in the range of the hyperfine parameters that were previously detected for nitrogen ligands coordinated to a Mn(III) ion. In contrast, the A_{iso} values of N_2 of ±3.0 and ±3.5 MHz in the absence and presence of azide, respectively, are in agreement with the A_{iso} values that have previously been determined for nitrogen ligands that are coordinated to a Mn(IV) ion. Thus, we assign the nitrogen atom N_1 to the His69 ligand that is coordinated to the Mn(III) ion and the nitrogen atom N_2 to His181 that is coordinated to the Mn(IV) ion of the Mn(III)−Mn(IV) center of manganese catalase. The hyperfine parameters that are obtained for the terminal nitrogen atom of the azide ion, N_3^-, that is coordinated to the Mn(III) ion in place of the water ligand provides additional support for this assignment. The smaller magnitude of A_{iso} and much larger value of $K^2(3 + \eta^2)$ provide evidence that the nitrogen atom of the azide ion is coordinated to the Mn(III) ion in an equatorial position. Since the nitrogen atom N_1 has a much larger A_{iso} component and $K^2(3 + \eta^2)$ that is 2 times smaller, we conclude that N_1 is an axial ligand of the Mn(III) ion. In contrast, the values of both A_{iso} and $K^2(3 + \eta^2)$ are small for the nitrogen atom N_2 which does not match the values for axial or equatorial coordination to the Mn(III) ion. The hyperfine parameters for the nitrogen atoms N_1 and N_2 are in agreement with previous reports in the literature.[87,89] The previous studies had tentatively assigned the nitrogen atom N_1 to an imino nitrogen atom coordinated to the Mn(III) ion and the nitrogen atom N_2 to an imino nitrogen atom coordinated to the Mn(IV) ion. Here, we confirm the assignment with additional hyperfine parameters that are obtained for the directly coordinated N_3^- ion in azide-treated manganese catalase.

Relation to Structure of Manganese Catalase and the OEC of Photosystem II. On the basis of the hyperfine parameters obtained from 2D ^1H and ^{14}N HYSCORE spectroscopy, we can draw important conclusions on the structure of superoxidized manganese catalase and the S_2 state of the OEC of PSII. Our experiments provide direct evidence that the water molecule and His69 and Glu35 residues in the dimanganese center of manganese catalase are coordinated to a manganese ion in the Mn(III) oxidation state. The second manganese ion, which is in the Mn(IV) oxidation state, is coordinated by the His181 and Glu148 residues. The magnitude of the anisotropic component, T, of the hyperfine interaction for the H_1 group of protons of the water ligand is only consistent with a Mn(III) oxidation state of the coordinating ion. Typically, the value of T is much smaller for a water molecule that is coordinated to a Mn(IV) ion.[76] We can exclude the existence of two isomeric forms of manganese catalase with interchanged oxidation states, since only one type of coupling is observed for each of the histidine ligands, His69 and His181. Moreover, the hyperfine parameters that are observed for the nitrogen atom N_3 of the N_3^- ion are in agreement with nearly equatorial coordination to a Mn(III) ion. The hyperfine parameters that are observed for the nitrogen atom N_1 of the His69 residue are in agreement with nearly axial coordination to a Mn(III) ion. In contrast, there is a large difference between the values of A_{iso} and $K^2(3 + \eta^2)$ for the nitrogen atoms N_1 and N_3, which suggests that the Jahn−Teller distortion axis of the Mn(III) ion is directed approximately along the His69 residue and one of the μ-oxo bridges in the dimanganese center. In contrast to the pure axial and equatorial ligands of the synthetic dimanganese models, the hyperfine parameters that are obtained for the nitrogen atoms N_1 and N_3 correspond to a distorted coordination geometry that likely arises from large steric effects of the bulky amino acid residues in the active site of manganese catalase.

Using a simple point-dipole approximation and the spin projection factor for a Mn(III) ion in mixed-valence Mn(III)−Mn(IV) centers ($p_{Mn(III)} = 2$),[75] we can estimate the distance between the metal ion and the H_1 and H_2 groups of protons. This calculation yields a center-to-center distance of 2.87 and 3.06 Å for the water protons and the proximal proton of His69, respectively. The estimated distances are in excellent agreement with the X-ray crystal structure of oxidized manganese catalase in the Mn(III)−Mn(III) form (distances of ∼2.8 and 3.06 Å, respectively).[88] This indicates that the dinuclear manganese center in the active site of manganese catalase does not undergo significant rearrangement upon transition to the superoxidized state.

In contrast with the dinuclear manganese center of manganese catalase, the OEC of PSII is comprised of four manganese ions and one calcium ion.[7] Despite this difference, there are important structural similarities between the metal center of superoxidized manganese catalase and the S_2 state of the OEC of PSII. Both centers have (i) Mn(III)−Mn(IV) di-μ-oxo structural unit(s), (ii) directly coordinated histidine ligand(s), (iii) directly coordinated water ligand(s), and (iv) a bulky proteinaceous environment compared to the smaller synthetic dimanganese models. These structural similarities make superoxidized manganese catalase an excellent model for

DOI: 10.1021/acs.jpcb.5b01602
J. Phys. Chem. B XXXX, XXX, XXX−XXX

the S_2 state of the OEC of PSII. A comparison of the spectroscopic properties of the two systems can provide new insight into the electronic structure of the OEC. As known from previous spectroscopic studies[104] and the recent 1.9 Å resolution X-ray crystal structure of PSII,[33] one of the manganese ions in the tetranuclear manganese calcium-oxo (Mn_4Ca-oxo) cluster, denoted as Mn1 in the X-ray crystal structure, is coordinated by the side chain of the D1-His332 residue. The hyperfine parameters of the nitrogen atom of D1-His332 that is directly coordinated to the Mn_4Ca-oxo cluster have been measured by multifrequency ESEEM[13] and 2D HYSCORE spectroscopy.[9] The values of A_{iso} and $K^2(3 + \eta^2)$ measured for the D1-His332 ligand in the S_2 state of the OEC are close to the values that are obtained for the His69 ligand in superoxidized manganese catalase. Thus, we suggest that the nature of the interaction between D1-His332 and the Mn1 ion in the S_2 state of the OEC is similar to the interaction between His69 and its coordinating Mn ion in superoxidized manganese catalase. Indeed, as observed for the His69 ligand in manganese catalase, the value of A_{iso} of D1-His332 is too large for a ligand of the Mn(IV) ion, and is much closer to the parameters that are observed for an axial (rather than equatorial) nitrogen ligand of a Mn(III) ion. The results that are obtained for manganese catalase in the present study indicate that quadrupolar parameters are a reliable probe of the coordination geometry of a Mn(III) ion even in the presence of steric restrictions that could induce significant distortions in the metal center. The quadrupolar parameter, $K^2(3 + \eta^2)$, that is measured for the D1-His332 residue in the S_2 state of the OEC of PSII is in agreement with that of His69 in superoxidized manganese catalase and the axial ligands of a Mn(III) ion in model systems.[80] Thus, in analogy with manganese catalase, it would be reasonable to conclude that the Mn1 ion in the S_2 state of the OEC is a Mn(III) center with a Jahn−Teller distortion axis approximately aligned with the direction of the Mn−N bond. This assignment also leads to the conclusion that the Mn1 ion is not oxidized in the S_1 to S_2 state transition, since it is widely accepted that the Mn_4Ca-oxo cluster in the OEC is comprised of two Mn(III) and two Mn(IV) ions in the S_1 state. Since the relative position of the metal ions remains virtually unchanged upon oxidation to the S_2 state of the OEC as observed by EXAFS spectroscopy, we also suggest that the electronic structure of the Mn1 ion is similar in both the S_1 and S_2 states of the OEC of PSII. In principle, the direction of the Jahn−Teller distortion axis can sometimes be located from the crystal structure based on the metal-to-ligand distances. However, the spectroscopic information described here is particularly valuable, as the relative position of the manganese ions in the X-ray crystal structure of PSII may be distorted by radiation damage of the cluster.[105]

Further details on the electronic structure of the S_2 state of the OEC of PSII can be derived by comparison of the proton hyperfine couplings of the dinuclear manganese center of manganese catalase. In recent investigations, we measured the hyperfine interaction of two proximal protons of the D1-His332 residue in the S_2 state of the OEC[8] and determined the value of the anisotropic hyperfine component, T, as ±4.4 MHz. This is smaller than the value that is measured for the proximal proton of the His69 residue, H_2, which is coordinated to the Mn(III) ion in superoxidized manganese catalase. The variation in the hyperfine parameters could either reflect differences in the metal-to-nucleus distances or differences in the spin projection factors for the respective Mn(III) ions. Unfortunately, the interatomic distances cannot be determined from the X-ray crystal structures of PSII. However, the similarity in the corresponding nitrogen hyperfine parameters makes it likely that the distances are similar. Assuming identical distances, we estimate the spin projection factor of the Mn1 ion, $p_{Mn1} = \pm 1.6$, using a spin projection factor for the Mn(III) ion in superoxidized manganese catalase, $p_{Mn(III)} = 2$, as expected for a strongly antiferromagnetically coupled Mn(III)−Mn(IV) center. Similarly, assuming identical coordination geometry of the water ligands, we can estimate the spin projection factor of the Mn4 ion that is coordinated to the two water ligands in the OEC of PSII. Since we obtained a value of T of ±4.1 MHz for the protons of the directly coordinated water(s) in the S_2 state of the OEC,[8] we calculate that the spin projection factor of the Mn4 ion, p_{Mn4}, is ±1.2. The values of p_{Mn1} and p_{Mn4} obtained here are slightly different from the values that were previously obtained using distances evaluated from the X-ray crystal structure PSII ($p_{Mn1} = \pm 1.9$ and $p_{Mn4} = \pm 1.1$).[7,68] Accurate determination of the spin projection factors is crucial for elucidating the electronic structure in the S_2 state of the OEC of PSII, since the spin projection factors are sensitive to the exchange coupling scheme of the four manganese ions in the Mn_4Ca-oxo cluster in the S_2 state. A range of values of $p_{Mn1} \sim 1.39-1.89$ and $p_{Mn4} \sim 0.75-1.02$ have been previously estimated from the ^{55}Mn hyperfine parameters that were obtained from ENDOR spectroscopy,[106] reflecting the spread of the intrinsic isotropic hyperfine parameters that have been reported in the literature for monomeric Mn(III) and Mn(IV) models. The authors of that study presented two coupling schemes for the OEC in the S_2 state. The first was based on a model proposed by Siegbahn, modified to be consistent with an $S = 1/2$ ground state.[2] In that scheme, the isotropic components of the spin projection tensors were calculated as $p_{Mn1} = 1.73$ and $p_{Mn4} = 1.11$ which are in agreement with the results of the present study. To obtain the second model, the authors used a coupling scheme based on the geometry of the Mn_4Ca-oxo cluster determined by EXAFS studies.[107] While the spin projection factor that was calculated for the Mn1 ion in that model, $p_{Mn1} = 1.84$, is in agreement with the present study, the spin projection factor that was previously calculated for the Mn4 ion, $p_{Mn4} = 0.87$, is smaller than the estimate in the present study. In an earlier study, Kulik and co-workers suggested two possible exchange coupling models of the OEC in the S_2 state.[108] The main difference between the two proposed models is the location of the unique Mn(III) ion in the Mn_4Ca-oxo cluster in the S_2 state of the OEC. In the first model, preferred by the authors, the Mn(III) ion is located at the "dangler position"; i.e., it is the Mn4 ion in the X-ray crystal structure. This model suggests values of p_{Mn1} and p_{Mn4} of 1.1 and 1.75, respectively, and does not agree with the estimate of the spin projection factors that are obtained in the present study. In the second model, the D1-His332 residue is coordinated to the Mn(III) ion, i.e., Mn1 in the X-ray crystal structure. The spin projection factors that are calculated for this model are $p_{Mn1} = 1.75$ and $p_{Mn4} = 1.1$, which are in excellent agreement with our experimental findings.

CONCLUSIONS

In this study, we use 2D HYSCORE spectroscopy to probe the electronic structure and ligand interactions of the mixed-valence Mn(III)−Mn(IV) core of superoxidized manganese catalase. We have determined that the water ligand is bound to the Mn(III) ion and confirmed that His69 and His181 are

DOI: 10.1021/acs.jpcb.5b01602
J. Phys. Chem. B XXXX, XXX, XXX−XXX

coordinated to Mn(III) and Mn(IV) centers, respectively, in a distorted axial geometry. These experimental observations provide several valuable insights into the electronic structure of the OEC of PSII in the S_2 state: (1) the histidine ligand D1-His332 is coordinated to manganese ion in the oxidation state Mn(III) in a distorted axial geometry, and (2) the spin projection factors of Mn1 and Mn4 ions of the OEC in the S_2 state are $\rho = \pm 1.6$ and $\rho = \pm 1.2$, respectively.

■ ASSOCIATED CONTENT

Supporting Information

The electron-spin-echo field-sweep EPR spectrum of superoxidized azide-treated manganese catalase in protonated buffer, the 2D HYSCORE spectra of superoxidized manganese catalase in deuterated buffer and superoxidized azide-treated manganese catalase in protonated buffer, the 2D ^{1}H HYSCORE spectrum of superoxidized azide-treated manganese catalase in protonated buffer, and the frequency-squared 2D ^{1}H HYSCORE spectrum of superoxidized manganese catalase in protonated buffer. This material is available free of charge via the Internet at http://pubs.acs.org.

■ AUTHOR INFORMATION

Corresponding Author

*Phone: (518) 698 7976. Fax: (518) 276 4887. E-mail: lakshk@rpi.edu.

Present Address

§(R.C.) Physical Biosciences Division, Lawrence Berkeley National Laboratory, Berkeley, CA 94720.

Notes

The authors declare no competing financial interest.

■ ACKNOWLEDGMENTS

This research is supported by the Photosynthetic Systems Program, Office of Basic Energy Sciences, United States Department of Energy (DE-FG02-07ER15903) (K.V.L.) and the National Institutes of Health (GM42680) (J.W.W.).

■ REFERENCES

(1) McEvoy, J. P.; Brudvig, G. W. Water-splitting Chemistry of Photosystem II. *Chem. Rev.* **2006**, *106*, 4455−4483.

(2) Siegbahn, P. E. M. Structures and Energetics for O_2 Formation in Photosystem II. *Acc. Chem. Res.* **2009**, *42*, 1871−1880.

(3) Kern, J.; Renger, G. Photosystem II: Structure and Mechanism of the Water: Plastoquinone Oxidoreductase. *Photosynth. Res.* **2007**, *94*, 183−202.

(4) Debus, R. J. The Manganese and Calcium Ions of Photosynthetic Oxygen Evolution. *Biochim. Biophys. Acta* **1992**, *1102*, 269−352.

(5) Yachandra, V. K.; Sauer, K.; Klein, M. P. Manganese Cluster in Photosynthesis: Where Plants Oxidize Water to Dioxygen. *Chem. Rev.* **1996**, *96*, 2927−2950.

(6) Kok, B.; Forbush, B.; McGloin, M. Cooperation of Charges in Photosynthetic O_2 Evolution - A Linear 4-Step Mechanism. *J. Photochem. Photobiol.* **1970**, *11*, 457−475.

(7) Umena, Y.; Kawakami, K.; Shen, J.-R.; Kamiya, N. Crystal Structure of Oxygen-evolving Photosystem II at a Resolution of 1.9 Angstrom. *Nature* **2011**, *473*, 55−65.

(8) Milikisiyants, S.; Chatterjee, R.; Coates, C. S.; Koua, F. H. M.; Shen, J. R.; Lakshmi, K. V. The Structure and Activation of Substrate Water Molecules in the S_2 State of Photosystem II Studied by Hyperfine Sublevel Correlation Spectroscopy. *Energy Environ. Sci.* **2012**, *5*, 7747−7756.

(9) Milikisiyants, S.; Chatterjee, R.; Weyers, A.; Meenaghan, A.; Coates, C.; Lakshmi, K. V. Ligand Environment of the S_2 State of Photosystem II: A Study of the Hyperfine Interactions of the Tetranuclear Manganese Cluster by 2D ^{14}N HYSCORE Spectroscopy. *J. Phys. Chem. B* **2010**, *114*, 10905−10911.

(10) Peloquin, J. M.; Campbell, K. A.; Randall, D. W.; Evanchik, M. A.; Pecoraro, V. L.; Armstrong, W. H.; Britt, R. D. ^{55}Mn ENDOR of the S_2 State Multiline EPR Signal of Photosystem II: Implications on the Structure of the Tetranuclear Manganese Cluster. *J. Am. Chem. Soc.* **2000**, *122*, 10926−10942.

(11) Randall, D. W.; Sturgeon, B. E.; Ball, J. A.; Lorigan, G. A.; Chan, M. K.; Klein, M. P.; Armstrong, W. H.; Britt, R. D. ^{55}Mn ESE-ENDOR of a Mixed-valence Mn(III)Mn(IV) Complex - Comparison with the Manganese Cluster of the Photosynthetic Oxygen-evolving Complex. *J. Am. Chem. Soc.* **1995**, *117*, 11780−11789.

(12) Tang, X. S.; Sivaraja, M.; Dismukes, G. C. Protein and Substrate Coordination to the Manganese Cluster in the Photosynthetic Water Oxidizing Complex - ^{15}N and ^{1}H ENDOR Spectroscopy of the S_2 State Multiline Signal in the Thermophilic Cyanobacterium *Synechococcus elongatus*. *J. Am. Chem. Soc.* **1993**, *115*, 2382−2389.

(13) Yeagle, G. J.; Gilchrist, M. L.; McCarrick, R. M.; Britt, R. D. Multifrequency Pulsed Electron Paramagnetic Resonance Study of the S_2 State of the Photosystem II Manganese Cluster. *Inorg. Chem.* **2008**, *47*, 1803−1814.

(14) Zouni, A.; Witt, H. T.; Kern, J.; Fromme, P.; Krauss, N.; Saenger, W.; Orth, P. Crystal Structure of Photosystem II from *Synechococcus elongatus* at 3.8 Angstrom Resolution. *Nature* **2001**, *409*, 739−743.

(15) Kamiya, N.; Shen, J. R. Crystal Structure of Oxygen-evolving Photosystem II from *Thermosynechococcus vulcanus* at 3.7 Angstrom Resolution. *Proc. Natl. Acad. Sci. U.S.A.* **2003**, *100*, 98−103.

(16) Ferreira, K. N.; Iverson, T. M.; Maghlaoui, K.; Barber, J.; Iwata, S. Architecture of the Photosynthetic Oxygen-evolving Center. *Science* **2004**, *303*, 1831−1838.

(17) Loll, B.; Kern, J.; Saenger, W.; Zouni, A.; Biesiadka, J. Towards Complete Cofactor Arrangement in the 3.0 Angstrom Resolution Structure of Photosystem II. *Nature* **2005**, *438*, 1040−1044.

(18) Grabolle, M.; Haumann, M.; Muller, C.; Liebisch, P.; Dau, H. Rapid Loss of Structural Motifs in the Manganese Complex of Oxygenic Photosynthesis by X-ray Irradiation at 10−300 K. *J. Biol. Chem.* **2006**, *281*, 4580−4588.

(19) Dau, H.; Liebisch, P.; Haumann, M. The Structure of the Manganese Complex of Photosystem II in its Dark-stable S_1 State - EXAFS Results in Relation to Recent Crystallographic Data. *Phys. Chem. Chem. Phys.* **2004**, *6*, 4781−4792.

(20) Schiller, H.; Dittmer, J.; Iuzzolino, L.; Dorner, W.; Meyer-Klaucke, W.; Sole, V. A.; Nolting, H. F.; Dau, H. Structure and Orientation of the Oxygen-evolving Manganese Complex of Green Algae and Higher Plants Investigated by X-ray Absorption Linear Dichroism Spectroscopy on Oriented Photosystem II Membrane Particles. *Biochemistry* **1998**, *37*, 7340−7350.

(21) Haumann, M.; Muller, C.; Liebisch, P.; Iuzzolino, L.; Dittmer, J.; Grabolle, M.; Neisius, T.; Meyer-Klaucke, W.; Dau, H. Structural and Oxidation State Changes of the Photosystem II Manganese Complex in Four Transitions of the Water Oxidation Cycle (S_0 -> S_1, S_1 -> S_2, S_2 -> S_3, and S_3, S_4 -> S_0) Characterized by X-ray Absorption Spectroscopy at 20 K and Room Temperature. *Biochemistry* **2005**, *44*, 1894−1908.

(22) Dau, H.; Dittmer, J.; Iuzzolino, L.; Schiller, H.; Dorner, W.; Heinze, I.; Sole, V. A.; Nolting, H. F. X-ray Absorption Linear Dichroism Spectroscopy (XALDS) on the Photosystem II Manganese Complex: Radiation Damage and S_1 State K-edge Spectra. *J. Phys. IV* **1997**, *7*, 607−610.

(23) Yachandra, V. K.; Derose, V. J.; Latimer, M. J.; Mukerji, I.; Sauer, K.; Klein, M. P. Where Plants Make Oxygen - A Structural Model for the Photosynthetic Oxygen-evolving Manganese Cluster. *Science* **1993**, *260*, 675−679.

(24) Cinco, R. M.; Holman, K. L. M.; Robblee, J. H.; Yano, J.; Pizarro, S. A.; Bellacchio, E.; Sauer, K.; Yachandra, V. K. Calcium EXAFS Establishes the Mn-Ca Cluster in the Oxygen-evolving Complex of Photosystem II. *Biochemistry* **2002**, *41*, 12928−12933.

DOI: 10.1021/acs.jpcb.5b01602
J. Phys. Chem. B XXXX, XXX, XXX−XXX

(25) Muller, C.; Liebisch, P.; Barra, M.; Dau, H.; Haumann, M. The Location of Calcium in the Manganese Complex of Oxygenic Photosynthesis Studied by X-ray Absorption Spectroscopy at the Ca k-edge. *Phys. Scr.* **2005**, *T115*, 847−850.
(26) George, G. N.; Prince, R. C.; Cramer, S. P. The Manganese Site of the Photosynthetic Water-splitting Enzyme. *Science* **1989**, *243*, 789−791.
(27) Kimura, Y.; Mizusawa, N.; Ishii, A.; Ono, T. FTIR Detection of Structural Changes in a Histidine Ligand During S-state Cycling of the Photosynthetic Oxygen-evolving Complex. *Biochemistry* **2005**, *44*, 16072−16078.
(28) Chu, H. A.; Hillier, W.; Debus, R. J. Evidence that the C-terminus of the D1 Polypeptide of Photosystem II is Ligated to the Manganese Ion that Undergoes Oxidation During the S_1 to S_2 Transition: An Isotope-edited FTIR Study. *Biochemistry* **2004**, *43*, 3152−3166.
(29) Strickler, M. A.; Walker, L. M.; Hillier, W.; Debus, R. J. Evidence from Biosynthetically Incorporated Strontium and FTIR Difference Spectroscopy that the C-terminus of the D1 Polypeptide of Photosystem II Does Not Ligate Calcium. *Biochemistry* **2005**, *44*, 8571−8577.
(30) Debus, R. J.; Strickler, M. A.; Walker, L. M.; Hillier, W. No Evidence from FTIR Difference Spectroscopy that Aspartate-170 of the D1 Polypeptide Ligates a Manganese Ion that Undergoes Oxidation During the S_0 to S_1, S_1 to S_2, or S_2 to S_3 Transitions in Photosystem II. *Biochemistry* **2005**, *44*, 1367−1374.
(31) Derose, V. J.; Yachandra, V. K.; McDermott, A. E.; Britt, R. D.; Sauer, K.; Klein, M. P. The State of Manganese in the Photosynthetic Apparatus - Nitrogen Ligation to Manganese in the Photosynthetic Oxygen-evolving Complex - Continuous-wave and Pulsed EPR Studies of Photosystem II Prticles Containing ^{14}N or ^{15}N. *Biochemistry* **1991**, *30*, 1335−1341.
(32) Tang, X. S.; Diner, B. A. Biochemical and Spectroscopic Characterization of a New Oxygen-evolving Photosystem II Core Complex from the Cyanobacterium *Synechocystis* PCC 6803. *Biochemistry* **1994**, *33*, 4594−4603.
(33) Umena, Y.; Kawakami, K.; Shen, J. R.; Kamiya, N. Crystal Structure of Oxygen-evolving Photosystem II at a Resolution of 1.9 Angstrom. *Nature* **2011**, *473*, 55−U65.
(34) Britt, R. D.; Peloquin, J. M.; Campbell, K. A. Pulsed and Parallel-polarization EPR Characterization of the Photosystem II Oxygen-evolving Complex. *Annu. Rev. Biophys. Biomol. Struct.* **2000**, *29*, 463−495.
(35) Britt, R. D.; Campbell, K. A.; Peloquin, J. M.; Gilchrist, M. L.; Aznar, C. P.; Dicus, M. M.; Robblee, J.; Messinger, J. Recent Pulsed EPR Studies of the Photosystem II Oxygen-evolving Complex: Implications as to Water Oxidation Mechanisms. *Biochim. Biophys. Acta, Bioenerg.* **2004**, *1655*, 158−171.
(36) Lohmiller, T.; Ames, W.; Lubitz, W.; Cox, N.; Misra, S. K. EPR Spectroscopy and the Electronic Structure of the Oxygen-evolving Complex of Photosystem II. *Appl. Magn. Reson.* **2013**, *44*, 691−720.
(37) Szalai, V. A.; Kuhne, H.; Lakshmi, K. V.; Brudvig, G. W. Characterization of the Interaction Between Manganese and Tyrosine-Z in Acetate-inhibited Photosystem II. *Biochemistry* **1998**, *37*, 13594−13603.
(38) Lakshmi, K. V.; Eaton, S. S.; Eaton, G. R.; Frank, H. A.; Brudvig, G. W. Analysis of Dipolar and Exchange Interactions Between Manganese and Tyrosine Z in the $S_2Y_Z^{\bullet}$ State of Acetate-inhibited Photosystem II Via EPR Spectral Simulations at X- and Q-bands. *J. Phys. Chem. B* **1998**, *102*, 8327−8335.
(39) Lakshmi, K. V.; Eaton, S. S.; Eaton, G. R.; Brudvig, G. W. Orientation of the Tetranuclear Manganese Cluster and Tyrosine-Z in the O_2-evolving Complex of Photosystem II: An EPR study of the $S_2Y_Z^{\bullet}$ State in Oriented Acetate-inhibited Photosystem II Membranes. *Biochemistry* **1999**, *38*, 12758−12767.
(40) Haddy, A.; Lakshmi, K. V.; Brudvig, G. W.; Frank, H. A. Q-band EPR of the S_2 State of Photosystem II Confirms an S = 5/2 Origin of the X-band g = 4.1 Signal. *Biophys. J.* **2004**, *87*, 2885−2896.
(41) Yamada, H.; Mino, H.; Itoh, S. Protons Bound to the Manganese Cluster in Photosystem II Oxygen-evolving Complex Detected by Proton Matrix ENDOR. *Biochim. Biophys. Acta, Bioenerg.* **2007**, *1767*, 197−203.
(42) Ahrling, K. A.; Peterson, S.; Styring, S. The S_0 State EPR Signal from the Mn Cluster in Photosystem II Arises from an Isolated S = 1/2 Ground State. *Biochemistry* **1998**, *37*, 8115−8120.
(43) Boussac, A.; Zimmermann, J. L.; Rutherford, A. W. Factors Influencing the Formation of Modified S_2 EPR Signal and the S_3 EPR Signal in Ca^{2+}-depleted Photosystem II. *FEBS Lett.* **1990**, *277*, 69−74.
(44) Dexheimer, S. L.; Klein, M. P. Detection of a Paramagnetic Intermediate in the S_1 State of the Photosynthetic Oxygen-evolving Complex. *J. Am. Chem. Soc.* **1992**, *114*, 2821−2826.
(45) Sarrou, J.; Ioannidis, N.; Deligiannakis, Y.; Petrouleas, V. A Mn(II)Mn(III) EPR Signal Arises from the Interaction of NO with the S_1 State of the Water-oxidizing Complex of Photosystem II. *Biochemistry* **1998**, *37*, 3581−3587.
(46) Ioannidis, N.; Nugent, J. H. A.; Petrouleas, V. Intermediates of the S_3 State of the Oxygen-evolving Complex of Photosystem II. *Biochemistry* **2002**, *41*, 9589−9600.
(47) Messinger, J.; Robblee, J. H.; Bergmann, U.; Fernandez, C.; Glatzel, P.; Visser, H.; Cinco, R. M.; McFarlane, K. L.; Bellacchio, E.; Pizarro, S. A.; et al. Absence of Mn-centered Oxidation in the S_2 -> S_3 Transition: Implications for the Mechanism of Photosynthetic Water Oxidation. *J. Am. Chem. Soc.* **2001**, *123*, 7804−7820.
(48) Maclachlan, D. J.; Nugent, J. H. A. Investigation of the S_3 Electron Paramagnetic Resonance Signal from the Oxygen-evolving Complex of Photosystem II - Effect of Inhibition of Oxygen Evolution by Acetate. *Biochemistry* **1993**, *32*, 9772−9780.
(49) Szalai, V. A.; Brudvig, G. W. Formation and Decay of the S_3 EPR Signal Species in Acetate-inhibited Photosystem II. *Biochemistry* **1996**, *35*, 1946−1953.
(50) Beck, W. F.; Depaula, J. C.; Brudvig, G. W. Active and Resting States of the O_2-evolving Complex of Photosystem II. *Biochemistry* **1985**, *24*, 3035−3043.
(51) Depaula, J. C.; Beck, W. F.; Brudvig, G. W. Magnetic Properties of Manganese in the Photosynthetic O_2-evolving Complex. 2. Evidence for a Manganese Tetramer. *J. Am. Chem. Soc.* **1986**, *108*, 4002−4009.
(52) Zheng, M.; Dismukes, G. C. Orbital Configuration of the Valence Electrons, Ligand Field Symmetry, and Manganese Oxidation States of the Photosynthetic Water Oxidizing Complex: Analysis of the S_2 State Multiline EPR Signals. *Inorg. Chem.* **1996**, *35*, 3307−3319.
(53) Brudvig, G. W. Structure and Function of Manganese in Photosystem II. In *Mechanistic Bioinorganic Chemistry*; Thorp, H. H., Pecoraro, V. L., Eds.; Advances in Chemistry Series; American Chemical Society: Washington, DC, 1995; Vol. *246*, pp 249−263.
(54) Brudvig, G. W. Involvement of Manganese in Photosynthetic Water Oxidation. *ACS Symp. Ser.* **1988**, *372*, 221−237.
(55) Boussac, A.; Rutherford, A. W. Comparative Study of the g = 4.1 EPR Signals in the S_2 State of Photosystem II. *Biochim. Biophys. Acta, Bioenerg.* **2000**, *1457*, 145−156.
(56) Boussac, A.; Girerd, J. J.; Rutherford, A. W. Conversion of the Spin State of the Manganese Complex in Photosystem II Induced by Near-infrared Light. *Biochemistry* **1996**, *35*, 6984−6989.
(57) Boussac, A.; Un, S.; Horner, O.; Rutherford, A. W. High-spin States ($S \geq 5/2$) of the Photosystem II Manganese Complex. *Biochemistry* **1998**, *37*, 4001−4007.
(58) Haddy, A.; Dunham, W. R.; Sands, R. H.; Aasa, R. Multifrequency EPR Investigations into the S_2 State Signal at g = 4 of the O_2-evolving Complex. *Biochim. Biophys. Acta* **1992**, *1099*, 25−34.
(59) Kim, D. H.; Britt, R. D.; Klein, M. P.; Sauer, K. The Manganese Site of the Photosynthetic Oxygen-evolving Complex Probed by EPR Spectroscopy of Oriented Photosystem II Membranes - The g = 4 and g = 2 Multiline Signals. *Biochemistry* **1992**, *31*, 541−547.
(60) Kim, D. H.; Britt, R. D.; Klein, M. P.; Sauer, K. The g = 4.1 EPR Signal of the S_2 State of the Photosynthetic Oxygen-evolving Complex

DOI: 10.1021/acs.jpcb.5b01602
J. Phys. Chem. B XXXX, XXX, XXX−XXX

Arises from a Multinuclear Manganese Cluster. *J. Am. Chem. Soc.* **1990**, *112*, 9389−9391.
(61) Haddy, A. EPR Spectroscopy of the Manganese Cluster of Photosystem II. *Photosynth. Res.* **2007**, *92*, 357−368.
(62) Dismukes, G. C.; Siderer, Y. EPR Spectroscopic Observations of a Manganese Center Associated with Water Oxidation in Spinach Chloroplasts. *FEBS Lett.* **1980**, *121*, 78−80.
(63) Dismukes, G. C.; Siderer, Y. Intermediates of a Polynuclear Manganese Center Involved in Photosynthetic Oxidation of Water. *Proc. Natl. Acad. Sci. U.S.A.* **1981**, *78*, 274−278.
(64) Peloquin, J. M.; Britt, R. D. EPR/ENDOR Characterization of the Physical and Electronic Structure of the OEC Manganese Cluster. *Biochim. Biophys. Acta, Bioenerg.* **2001**, *1503*, 96−111.
(65) Britt, R. D.; Zimmermann, J. L.; Sauer, K.; Klein, M. P. The State of Manganese in the Photosynthetic Apparatus. 10. Ammonia Binds to the Catalytic Mn of the Oxygen-evolving Complex of Photosystem II - Evidence by Electron-Spin Echo Envelope Modulation Spectroscopy. *J. Am. Chem. Soc.* **1989**, *111*, 3522−3532.
(66) Stich, T. A.; Yeagle, G. J.; Service, R. J.; Debus, R. J.; Britt, R. D. Ligation of D1-His332 and D1-Asp170 to the Manganese Cluster of Photosystem II from *Synechocystis* Assessed by Multifrequency Pulse EPR Spectroscopy. *Biochemistry* **2011**, *50*, 7390−7404.
(67) Tang, X. S.; Diner, B. A.; Larsen, B. S.; Gilchrist, M. L.; Lorigan, G. A.; Britt, R. D. Identification of Histidine at the Catalytic Site of the Photosynthetic Oxygen-evolving Complex. *Proc. Natl. Acad. Sci. U.S.A.* **1994**, *91*, 704−708.
(68) Chatterjee, R.; Milikisiyants, S.; Coates, C. S.; Koua, F. M. K.; Shen, J.-R.; Lakshmi, K. V. The Structure and Activation of Substrate Water Molecules in Sr^{2+}-substituted Photosystem II. *Phys. Chem. Chem. Phys.* **2014**, *16*, 20834−20843.
(69) Kawamori, A.; Inui, T.; Ono, T.; Inoue, Y. ENDOR Study on the Position of Hydrogens Close to the Manganese Cluster in S_2 State of Photosystem II. *FEBS Lett.* **1989**, *254*, 219−224.
(70) Fiege, R.; Zweygart, W.; Bittl, R.; Adir, N.; Renger, G.; Lubitz, W. EPR and ENDOR Studies of the Water Oxidizing Complex of Photosystem II. *Photosynth. Res.* **1996**, *48*, 227−237.
(71) Aznar, C. P.; Britt, R. D. Simulations of the ^{1}H Electron Spin Echo-Electron Nuclear Double Resonance and ^{2}H Electron Spin Echo Envelope Modulation Spectra of Exchangeable Hydrogen Nuclei Coupled to the S_2 State Photosystem II Manganese Cluster. *Philos. Trans. R. Soc. London, Ser. B* **2002**, *357*, 1359−1365.
(72) Su, J.-H.; Messinger, J. Is Mn-Bound Substrate Water Protonated in the S_2 State of Photosystem II? *Appl. Magn. Reson.* **2010**, *37*, 123−136.
(73) Mukhopadhyay, S.; Mandal, S. K.; Bhaduri, S.; Armstrong, W. H. Manganese Clusters with Relevance to Photosystem II. *Chem. Rev.* **2004**, *104*, 3981−4026.
(74) Zweygart, W.; Bittl, R.; Wieghardt, K.; Lubitz, W. EPR and ^{55}Mn *cw* ENDOR Study of an Antiferrogmagnetically Coupled Dinuclear Manganese (Mn(IV)Mn(III)) Complex. *Chem. Phys. Lett.* **1996**, *261*, 272−276.
(75) Randall, D. W.; Chan, M. K.; Armstrong, W. H.; Britt, R. D. Pulsed ^{1}H and ^{55}Mn ENDOR Studies of Dinuclear Mn(III)Mn(IV) Model Complexes. *Mol. Phys.* **1998**, *95*, 1283−1294.
(76) Milikisiyants, S.; Chatterjee, R.; Lakshmi, K. V. Two-Dimensional ^{1}H HYSCORE Spectroscopy of Dimanganese Di-μ-oxo Mimics of the Oxygen-Evolving Complex of Photosystem II. *J. Phys. Chem. B* **2011**, *115*, 12220−12229.
(77) Schafer, K. O.; Bittl, R.; Zweygart, W.; Lendzian, F.; Haselhorst, G.; Weyhermuller, T.; Wieghardt, K.; Lubitz, W. Electronic Structure of Antiferromagnetically Coupled Dinuclear Manganese (Mn(IV)Mn(III)) Complexes Studied by Magnetic Resonance Techniques. *J. Am. Chem. Soc.* **1998**, *120*, 13104−13120.
(78) Randall, D. W.; Gelasco, A.; Caudle, M. T.; Pecoraro, V. L.; Britt, R. D. ESE-ENDOR and ESEEM Characterization of Water and Methanol Ligation to a Dinuclear Mn(III)Mn(IV) Complex. *J. Am. Chem. Soc.* **1997**, *119*, 4481−4491.
(79) Tan, X. L.; Gultneh, Y.; Sarneski, J. E.; Scholes, C. P. EPR-ENDOR of the Electronic Structure from Two Nitrogenously Ligated Bis(μ-oxo)-MnIII-MnIV Model Complexes Spectroscopically Relevant to the Multi-manganese Center of Photosystem II. *J. Am. Chem. Soc.* **1991**, *113*, 7853−7858.
(80) Chatterjee, R.; Milikisiyants, S.; Lakshmi, K. V. Two-dimensional ^{14}N HYSCORE Spectroscopy of the Coordination Geometry of Ligands in Dimanganese Di-μ-oxo Mimics of the Oxygen-evolving Complex of Photosystem II. *Phys. Chem. Chem. Phys.* **2012**, *14*, 7090−7097.
(81) Campbell, K. A.; Force, D. A.; Nixon, P. J.; Dole, F.; Diner, B. A.; Britt, R. D. Dual-mode EPR Detects the Initial Intermediate in Photoassembly of the Photosystem II Mn Cluster: The Influence of Amino Acid Residue 170 of the D1 Polypeptide on Mn Coordination. *J. Am. Chem. Soc.* **2000**, *122*, 3754−3761.
(82) Yamaguchi, K.; Yamanaka, S.; Isobe, H.; Saito, T.; Kanda, K.; Umena, Y.; Kawakami, K.; Shen, J. R.; Kamiya, N.; Okumura, M.; et al. The Nature of Chemical Bonds of the $CaMn_4O_5$ Cluster in Oxygen-evolving Complex of Photosystem II: Jahn-Teller Distortion and its Suppression by Ca Doping in Cubane Structures. *Int. J. Quantum Chem.* **2013**, *113*, 453−473.
(83) Yamaguchi, K.; Isobe, H.; Yamanaka, S.; Saito, T.; Kanda, K.; Shoji, M.; Umena, Y.; Kawakami, K.; Shen, J. R.; Kamiya, N.; et al. Full Geometry Optimizations of the Mixed-valence $CaMn_4O_4X(H2O)_4$ (X = OH or O) Cluster in OEC of PSII: Degree of Symmetry Breaking of the Labile Mn-X-Mn Bond Revealed by Several Hybrid DFT Calculations. *Int. J. Quantum Chem.* **2013**, *113*, 525−541.
(84) Pantazis, D. A.; Orio, M.; Petrenko, T.; Zein, S.; Lubitz, W.; Messinger, J.; Neese, F. Structure of the Oxygen-evolving Complex of Photosystem II: Information on the S_2 State Through Quantum Chemical Calculation of its Magnetic Properties. *Phys. Chem. Chem. Phys.* **2009**, *11*, 6788−6798.
(85) Waldo, G. S.; Yu, S. Y.; Pennerhahn, J. E. Structural Characterization of the Binuclear Mn Site in *Lactobacillus plantarum* Manganese Catalase. *J. Am. Chem. Soc.* **1992**, *114*, 5869−5870.
(86) McConnell, I. L.; Grigoryants, V. M.; Scholes, C. P.; Myers, W. K.; Chen, P. Y.; Whittaker, J. W.; Brudvig, G. W. EPR-ENDOR Characterization of (^{17}O, ^{1}H, ^{2}H) Water in Manganese Catalase and Its Relevance to the Oxygen-evolving Complex of Photosystem II. *J. Am. Chem. Soc.* **2012**, *134*, 1504−1512.
(87) Stich, T. A.; Whittaker, J. W.; Britt, R. D. Multifrequency EPR Studies of Manganese Catalases Provide a Complete Description of Protenaceous Nitrogen Coordination. *J. Phys. Chem. B* **2010**, *114*, 14178−14188.
(88) Barynin, V. V.; Whittaker, M. M.; Antonyuk, S. V.; Lamzin, V. S.; Harrison, P. M.; Artymiuk, P. J.; Whittaker, J. W. Crystal Structure of Manganese Catalase from *Lactobacillus plantarum*. *Structure* **2001**, *9*, 725−738.
(89) Stemmler, T. L.; Sturgeon, B. E.; Randall, D. W.; Britt, R. D.; PennerHahn, J. E. Spectroscopic Characterization of Inhibitor Interactions with the Mn(III)Mn(IV) Core in *Lactobacillus plantarum* Manganese Catalase. *J. Am. Chem. Soc.* **1997**, *119*, 9215−9225.
(90) Khangulov, S.; Sivaraja, M.; Barynin, V. V.; Dismukes, G. C. The Dimanganese (III,IV) Oxidation-state of Catalase from *Thermus thermophilus* - Electron Nuclear Double-Resonance Analysis of Water and Protein Ligands in the Active Site. *Biochemistry* **1993**, *32*, 4912−4924.
(91) Whittaker, M.; Barynin, V.; Igarashi, T.; Whittaker, J. Outer Sphere Mutagenesis of *Lactobacillus plantarum* Manganese Catalase Disrupts the Cluster Core. *Eur. J. Biochem.* **2003**, *270*, 1102−1116.
(92) Waldo, G. S.; Fronko, R. M.; Pennerhahn, J. E. Inactivation and Reactivation of Manganese Catalase - Oxidation State Assignments using X-Ray Absorption Spectroscopy. *Biochemistry* **1991**, *30*, 10486−10490.
(93) Waldo, G. S.; Pennerhahn, J. E. Mechanism of Manganese Catalase Peroxide Disproportionation - Determination of Manganese Oxidation States During Turnover. *Biochemistry* **1995**, *34*, 1507−1512.
(94) Khangulov, S. V.; Barynin, V. V.; Antonyukbarynina, S. V. Manganese-containing Catalase from *Thermus thermophilus* Peroxide-induced Redox Transformation of Manganese Ions in Presence of

DOI: 10.1021/acs.jpcb.5b01602
J. Phys. Chem. B XXXX, XXX, XXX−XXX

Specific Inhibitors of Catalase Activity. *Biochim. Biophys. Acta* **1990**, *1020*, 25−33.
(95) Kasumaj, B.; Stoll, S. 5- and 6-pulse Electron Spin Echo Envelope Modulation (ESEEM) of Multi-nuclear Spin Systems. *J. Magn. Reson.* **2008**, *190*, 233−247.
(96) Song, R.; Zhong, Y. C.; Noble, C. J.; Pilbrow, J. R.; Hutton, D. R. A New 6-pulse Two-dimensional Electron-spin Echo Envelope Modulation (ESEEM) Correlation Spectroscopy. *Chem. Phys. Lett.* **1995**, *237*, 86−90.
(97) Dikanov, S. A.; Bowman, M. K. Cross-peak Lineshape of Two-dimensional ESEEM Spectra in Disordered S = 1/2, I = 1/2 Spin Systems. *J. Magn. Reson., Ser. A* **1995**, *116*, 125−128.
(98) Cooper, S. R.; Dismukes, G. C.; Klein, M. P.; Calvin, M. Mixed-valence Interactions in Di-μ-oxo Bridged Manganese Complexes - Electron Paramagnetic Resonance and Magnetic Susceptibility Studies. *J. Am. Chem. Soc.* **1978**, *100*, 7248−7252.
(99) Brewer, K. J.; Calvin, M.; Lumpkin, R. S.; Otvos, J. W.; Spreer, L. O. Synthesis, Structure and Characterization of a Mixed-valence Manganese(III)-Manganese(IV) Bis(μ-oxo) Complex with a Macrocyclic Tetraaza Ligand. *Inorg. Chem.* **1989**, *28*, 4446−4451.
(100) Schafer, K. O.; Bittl, R.; Lendzian, F.; Barynin, V.; Weyhermuller, T.; Wieghardt, K.; Lubitz, W. Multifrequency EPR Investigation of Dimanganese Catalase and Related Mn(III)Mn(IV) Complexes. *J. Phys. Chem. B* **2003**, *107*, 1242−1250.
(101) Ivancich, A.; Barynin, V. V.; Zimmermann, J. L. Pulsed EPR Studies of the Binuclear Mn(III)Mn(IV) Center in Catalase from *Thermus thermophilus*. *Biochemistry* **1995**, *34*, 6628−6639.
(102) Brudvig, G. W.; Casey, J. L.; Sauer, K. The Effect of Temperature on the Formation and Decay of the Multiline EPR Signal Species Associated with Photosynthetic Oxygen Evolution. *Biochim. Biophys. Acta* **1983**, *723*, 366−371.
(103) Hofer, P.; Grupp, A.; Nebenfuhr, H.; Mehring, M. Hyperfine Sublevel Correlation (HYSCORE) Spectroscopy - A 2D Electron Spin Resonance Investigation of the Squaric Acid Radical. *Chem. Phys. Lett.* **1986**, *132*, 279−282.
(104) Debus, R. J.; Campbell, K. A.; Gregor, W.; Li, Z. L.; Burnap, R. L.; Britt, R. D. Does Histidine-332 of the D1 Polypeptide Ligate the Manganese Cluster in Photosystem II? An Electron Spin Echo Envelope Modulation Study. *Biochemistry* **2001**, *40*, 3690−3699.
(105) Galstyan, A.; Robertazzi, A.; Knapp, E. W. Oxygen-evolving Mn Cluster in Photosystem II: The Protonation Pattern and Oxidation State in the High-resolution Crystal Structure. *J. Am. Chem. Soc.* **2012**, *134*, 7442−7449.
(106) Cox, N.; Rapatskiy, L.; Su, J. H.; Pantazis, D. A.; Sugiura, M.; Kulik, L.; Dorlet, P.; Rutherford, A. W.; Neese, F.; Boussac, A.; et al. Effect of Ca^{2+}/Sr^{2+} Substitution on the Electronic Structure of the Oxygen-evolving Complex of Photosystem II: A Combined Multifrequency EPR, ^{55}Mn ENDOR, and DFT Study of the S_2 State. *J. Am. Chem. Soc.* **2011**, *133*, 3635−3648.
(107) Yano, J.; Kern, J.; Sauer, K.; Latimer, M. J.; Pushkar, Y.; Biesiadka, J.; Loll, B.; Saenger, W.; Messinger, J.; Zouni, A.; et al. Where Water is Oxidized to Dioxygen: Structure of the Photosynthetic Mn_4Ca Cluster. *Science* **2006**, *314*, 821−825.
(108) Kulik, L. V.; Epel, B.; Lubitz, W.; Messinger, J. Electronic Structure of the Mn_4Oxo-Ca Cluster in the S_0 and S_2 States of the Oxygen-evolving Complex of Photosystem II Based on Pulse ^{55}Mn ENDOR and EPR Spectroscopy. *J. Am. Chem. Soc.* **2007**, *129*, 13421−13435.

DOI: 10.1021/acs.jpcb.5b01602
J. Phys. Chem. B XXXX, XXX, XXX−XXX